Article

Crystal Structures, Electronic Properties, and Pressure-Induced Superconductivity of the Tetrahedral Cluster Compounds GaNbS, GaNbSe, and GaTaSe

Regina Pocha, Dirk Johrendt, Bingfang Ni, and Mohsen M. Abd-Elmeguid

J. Am. Chem. Soc., **2005**, 127 (24), 8732-8740• DOI: 10.1021/ja050243x • Publication Date (Web): 27 May 2005

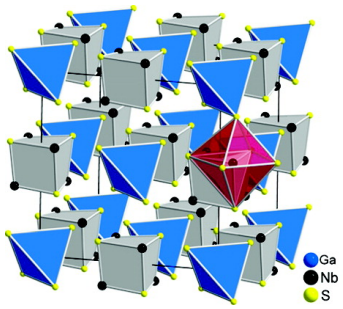

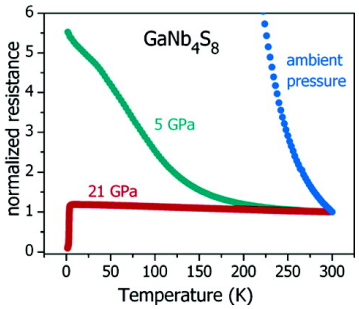

More About This Article

Additional resources and features associated with this article are available within the HTML version:

- Supporting Information
- Links to the 8 articles that cite this article, as of the time of this article download
- Access to high resolution figures
- Links to articles and content related to this article
- Copyright permission to reproduce figures and/or text from this article

View the Full Text HTML

J|A|C|S
ARTICLES
Published on Web 05/27/2005

Crystal Structures, Electronic Properties, and Pressure-Induced Superconductivity of the Tetrahedral Cluster Compounds $GaNb_4S_8$, $GaNb_4Se_8$, and $GaTa_4Se_8$

Regina Pocha, Dirk Johrendt,*,† Bingfang Ni,‡ and Mohsen M. Abd-Elmeguid‡

Contribution from the Department Chemie and Biochemie der Ludwig-Maximilians-Universität München, Butenandtstrasse 5-13 (Haus D), 81377 München, Germany, and II. Physikalisches Institut, Universität zu Köln, Zülpicher Strasse 77, 50937 Köln, Germany

Received January 13, 2005; E-mail: Dirk.Johrendt@cup.uni-muenchen.de

Abstract: The crystal structures of the tetrahedral cluster compounds $GaNb_4S_8$ and $GaTa_4Se_8$ were determined by single-crystal X-ray diffraction. They crystallize in the cubic $GaMo_4S_8$ structure type ($F\bar{4}3m$), which can be derived from the spinel type by shifting the metal atoms off the centers of the chalcogen octahedra along [111]. Electrical resistivity and magnetic susceptibility measurements show that the electronic conduction originates from hopping of localized unpaired electrons ($S = {}^1/_2$) among widely separated Nb_4 or Ta_4 clusters, and thus these materials represent a new class of Mott insulators. Under high pressure we find that $GaNb_4S_8$ undergoes a transition from the Mott insulating to a superconducting state with T_C up to 4 K at 23 GPa, similar to $GaNb_4Se_8$ and $GaTa_4Se_8$. High-pressure single-crystal X-ray studies of $GaTa_4Se_8$ reveal that the superconducting transition is connected with a gradual decrease of the octahedral distortion with increasing pressure. DFT band structure calculations show that weakly coupled cluster orbitals are responsible for a high density of states at the Fermi level. The correct insulating magnetic ground state for $GaNb_4S_8$ with $\mu_{eff} = 1.73\ \mu_B$ is for the first time achieved by the LDA+U method using $U = 6$ eV and rhombohedral symmetry.

1. Introduction

The investigation of the physical properties of matter at the borderline between the metallic and nonmetallic state has attracted much interest over decades.[1] This is due to the fact that the ground-state properties in this area are determined by strong electronic correlation effects. A so-called Mott- or Coulomb-blockaded insulator is a material where the electrons are localized because the energy cost incurred if one electron were to move on to a neighboring site (where it interacts with already resident electrons) is too high relative to the available electronic kinetic energy for this transfer to occur. The energy required for this hopping process is called the Hubbard U, which is defined as $I - A$, where I is the ionization energy to remove an electron from one ion and A is the electron affinity gained when the electron is added to another site. These findings were first reported in pioneering works of De Boer,[2] Peierls,[3] Mott,[4,5] and Hubbard[6] and have experienced further importance in semiconductor research,[7] and particularly after the discovery of high-T_C superconductivity.[8] Usually, high-T_C superconductivity is obtained by doping Mott insulators[9] such as the well-known cuprates or other oxides.[10,11] On the other hand, transitions of stoichiometric Mott insulators to superconductors are extremely rare. It has thus been a challenging effort to search for Mott insulating systems in proximity to the metal-to-insulator transition (MIT).[1] In general, stoichiometric Mott insulators often exhibit very large activation energies[12] and are very difficult to be tuned to the MIT at applicable pressures. As an example, the MIT for NiO is theoretically expected at pressures in the TPa range.[13] On going to NiS with a much smaller activation energy, a MIT occurs already at ambient pressure ($T_t \approx 260$ K),[14] and NiSe is finally a metallic conductor throughout. This clearly shows that Mott insulating transition metal sulfides or selenides are very promising compounds by which to study the borderline between the metallic and the localized states of stoichiometric materials.

A further structural aspect introduces additional degrees of freedom in these systems, namely if the "correlated units" of the Mott insulator would not be single metal atoms with partially occupied d orbitals, but small metal cluster units with partially filled cluster-molecular orbitals. A suitable crystal structure to pursue this idea is known among chalcogenides of the so-called

† Ludwig-Maximilians-Universität München.
‡ Universität zu Köln.

(1) Imada, M.; Fujimori, A.; Tokura, Y. *Rev. Mod. Phys.* **1998**, *70*, 1039 and references therein.
(2) De Boer, J. H.; Verwey, E. J. W. *Proc. Phys. Soc.* **1937**, *49*, 59.
(3) Mott, N. F.; Peierls, R. *Proc. Phys. Soc.* **1937**, *49*, 72.
(4) Mott, N. F. *Proc. Phys. Soc.* **1949**, *62*, 416.
(5) Mott, N. F. *Rep. Prog. Phys.* **1984**, *47*, 909.
(6) Hubbard, J. *Proc. R. Soc.* **1964**, *277*, 237.
(7) Lerner, E. J. *IBM Res.* **1999**, Number 4.
(8) Anderson, P. W. *Science* **1987**, *235*, 4793; *Science* **1987**, *235*, 1196.
(9) Kivelson, S. A.; Emery, V. J. *Synth. Met.* **1996**, *80*, 151.
(10) Bednorz, J. G.; Müller, K. A. *Z. Phys. B* **1986**, *64*, 189.
(11) Yamauchi, T.; Ueda, Y.; Môri, N. *Phys. Rev. Lett.* **2002**, *89*, 57002-1.
(12) The activation energy is mainly determined by the effective hopping matrix element which includes the effective bandwidth of a given system.
(13) Feng, X.-B.; Harrison, N. M. *Phys Rev. B* **2004**, *69*, 35114.
(14) Komoto, T.; Sparks, J. T. *Phys. Lett. A* **1967**, *25*, 398.

10.1021/ja050243x CCC: $30.25

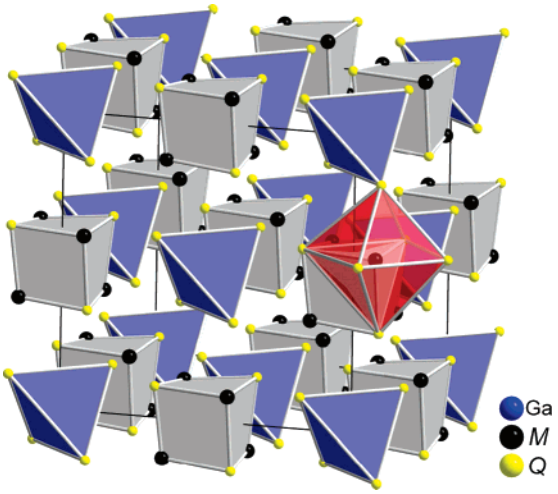

Figure 1. Crystal structure of GaM_4Q_8 with M = Nb, Ta; Q = S, Se ($GaMo_4S_8$-type). The rocksalt-like distribution of M_4Q_4 cubes and GaQ_4 tetrahedra is emphasized. The distorted octahedral coordination of the M atoms is also indicated in red.

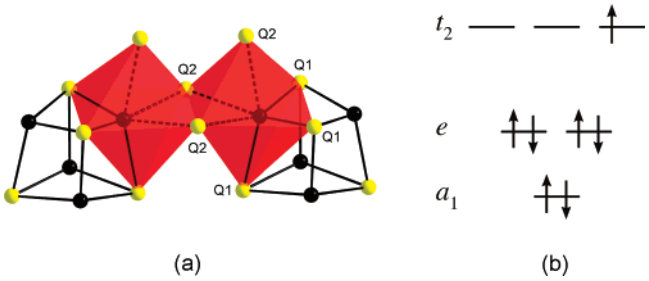

Figure 2. (a) Connection of two M_4Q_4 cubes in GaM_4Q_8. The M atoms (black spheres) are located in distorted, edge-sharing MQ_6 octahedra (red) with three shorter $M-Q1$ (solid) and three longer $M-Q2$ bonds (dashed). (b) MO scheme of the tetrahedral M_4-cluster with M = V, Nb, Ta, occupied by seven electrons according to the formula $GaM_4^{3.25+}Q_8^{2-}$.

$GaMo_4S_8$ type, which is depicted in Figure 1. The structure can be derived from the spinel type AM_2Q_4. Gallium occupies one-half of the tetrahedral sites (atom A) in the cubic close packing of Q atoms in an ordered way, which reduces the space group symmetry from $Fd\bar{3}m$ to $F\bar{4}3m$. The coordinates of the metal atom (M) are shifted along the three-fold axis (x,x,x) from $x = 0.625$ ($^5/_8$) to $x \approx 0.603$. This shift has important consequences: (i) the metal atoms are no longer in the centers of the chalcogen octahedra, but the distances split into three longer $M-Q1$ and three shorter $M-Q2$ bonds, as shown in Figure 2a. (ii) The metal atoms join to tetrahedral M_4 clusters with $M-M$ distances about 3 Å and intercluster $M\cdots M$ distances about 4.2 Å. This makes a description as a rocksalt-like arrangement of M_4Q_4 cubes and GaQ_4 tetrahedra appropriate, which is emphasized in Figure 1. However, the change in the metal atom positions is very important for the electronic properties of these materials.

The metal atoms in the spinel type form a three-dimensional network with each six metal neighbors, which is also known as the pyrochlore net. If the $M-M$ distances are not too long and the metal d shell is partially filled, one can expect metallic conductivity. Examples are several metallic thiospinel compounds such as CuM_2S_4, with M = V, Ir, Rh.[15] By joining the metal atoms to tetrahedral cluster units, electrons become localized in the cluster bonding states and are thereby no longer available for metallic conductivity. Thus, the $GaMo_4S_8$-type compounds are expected to be Mott−Hubbard insulators, but their correlated units are tetrahedral M_4 cluster units (or molecular orbitals [MOs]) instead of separate metal atoms. Hopping of carriers between these units is only possible if the cluster-MOs are partially occupied. According to MO theory, six $M-M$ bonding states are available in a M_4 cluster with T_d symmetry, as shown in Figure 2b. One a_1, one two-fold degenerate e, and one three-fold degenerated t_2 occur for a maximum electron count of 12.

Following our previous work about the magnetic Mott insulators AV_4Q_8 (A = Ga, Ge; Q = S, Se),[16,17] we have now directed our interest toward the isostructural compounds with 4d and 5d group 5 metals, niobium and tantalum. The corresponding M_4 cluster-MO is now occupied by only seven electrons with one unpaired spin in the t_2 level ($S = {}^1/_2$), as shown schematically in Figure 2b. $GaNb_4S_8$, $GaNb_4Se_8$, and $GaTa_4Se_8$ were first reported by Ben Yaich et al.,[18] who concluded that the observed weak paramagnetism is similar to those of intermetallic compounds with very high density of states, but they have not investigated the Mott insulating behavior. In contrast to this, one unpaired spin in $GaMo_4S_8$ with 11 electrons per Mo_4 causes ferromagnetic ordering at low temperatures.[19]

Recently, we have discovered pressure-induced transitions from the Mott insulating to a superconducting state in $GaTa_4Se_8$ and $GaNb_4Se_8$, beginning at ~10 GPa with T_C's up to 8 K.[20] In this work, we present comprehensive experimental and theoretical investigations of the structures and properties of this class of materials. We report the structural parameters of single crystals of $GaNb_4S_8$ and $GaTa_4Se_8$ together with the results of electrical resistivity and magnetic susceptibility measurements at ambient pressure. In addition, we show the effect of high pressure on the structural parameters of $GaTa_4Se_8$ and on the electronic conduction of $GaNb_4S_8$, which transforms likewise from the Mott insulating to a superconducting state under pressure. Because of the particular importance of the electronic structure in these compounds, we present the results of DFT band structure calculations to gain an insight in the electronic properties of this new class of Mott insulators from a chemical point of view.

2. Crystal structures

First we have determined the single-crystal structure data for $GaNb_4S_8$ and $GaTa_4Se_8$ at ambient pressure (which were not reported in ref 18) and then for $GaTa_4Se_8$ at pressures of 5, 10, and 14.5 GPa in the diamond-anvil cell (DAC). The necessary hydrostatic conditions are difficult to maintain above 10 GPa with N_2 as pressure medium. Therefore, we choose $GaTa_4Se_8$ for the high-pressure experiment because of its lowest com-

(15) (a) Maehl, D.; Pickardt, J.; Reuter, B. *Z. Anorg. Allg. Chem.* **1982**, *491*, 203. (b) Riedel, E.; Pickardt, J.; Soechtig, J. *Z. Anorg. Allg. Chem.* **1976**, *419*, 63. (c) Hagino, T.; Seki, Y.; Wada, N.; Tsuji, S.; Shirane, T.; Kumagai, K.; Nagata, S. *Phys. Rev. B* **1995**, *51*, 12673. (d) Furubayashi, T.; Matsumoto T.; Hagino, T.; Nagata, S. *J. Phys. Soc. Jpn.* **1004**, *63*, 3333.
(16) Johrendt, D. *Z. Anorg. Allg. Chem.* **1998**, *624*, 952.
(17) Pocha, R.; Johrendt, D.; Pöttgen, R. *Chem. Mater.* **2000**, *12*, 2882.
(18) Ben Yaich, H.; Jegaden, J. C.; Potel, M.; Sergent, M.; Rastogi, A. K.; Tournier, R. *J. Less-Common Met.* **1984**, *102*, 9.
(19) Shamrai, V.; Mädge, H.; Mydlarz, T.; Leitus, G. *J. Low Temp. Phys.* **1982**, *49*, 123.
(20) Abd-Elmeguid, M. M.; Ni, B.; Khomskii, D. I.; Pocha, R.; Johrendt, D.; Wang, X.; Syassen, K. *Phys. Rev. Lett.* **2004**, *93*, 126403−1.

Table 1. Crystal Structure Data of GaM_4Q_8 (M = Nb, Ta; Q = S, Se)

formula	$GaNb_4S_8$	$GaNb_4Se_8$[a]	$GaTa_4Se_8$			
fw (g/mol)	697.88	1073.03	1435.2			
space group, Z	$F\bar{4}3m$, 4	$F\bar{4}3m$, 4	$F\bar{4}3m$, 4			
λ (Å)	0.71073	0.71073	0.71073			
pressure (GPa)	ambient	ambient	ambient	5	10	14.5
a (Å)	9.985(2)	10.42	10.358(1)	10.201(1)	10.064(2)	9.994(5)
V (Å^3)	995.51	1131.37	1111.29	1061.52	1019.32	998.20
ρ (g/cm^3)	4.656	6.300	8.518	8.918	9.287	9.483
μ (mm^{-1})	8.75	31.96	67.7	70.9	73.9	75.4
ϑ range (deg)	3.5−35.0	−	3.4−42.8	3.5−24.3	3.5−22.4	3.5−22.4
no. indep. refl.	215	195	250	61	47	68
no. variables	9	-	9	9	7	7
R	0.021	0.049	0.073	0.069	0.076	0.096
R_w	0.019	0.050	0.029	0.023	0.033	0.067
			Atomic Positions[b]			
x (Ga)	0	0	0	0	0	0
x (M)	0.60535(4)	0.6031(3)	0.6025(1)	0.6030(3)	0.6035(5)	0.6036(5)
x ($Q1$)	0.3672(1)	0.3643(4)	0.3643(2)	0.3621(5)	0.3605(8)	0.3600(9)
x ($Q2$)	0.8671(1)	0.8656(4)	0.8646(2)	0.8655(4)	0.8662(8)	0.8666(8)
			Distances (Å)			
d_{M-M} (3×)	2.975(1)	3.026	3.002(2)	2.971(4)	2.945(6)	2.929(7)
$d_{M\cdots M}$ (3×)	4.085(1)	4.320	4.322(1)	4.243(4)	4.171(7)	4.137(7)
d_{M-Q1} (3×)	2.410(1)	2.526	2.515(2)	2.508(6)	2.498(9)	2.488(11)
d_{M-Q2} (3×)	2.642(1)	2.768	2.758(2)	2.717(5)	2.679(9)	2.662(10)
d_{Ga-Q2} (4×)	2.299(1)	2.418	2.429(2)	2.377(5)	2.332(8)	2.309(8)
D^{MM} (%)[c]	37	43	44	43	42	41
D^{MQ} (%)[d]	9.6	9.6	9.6	8.3	7.2	7.0

[a] Data for $GaNb_4Se_8$ are from ref 18. [b] Ga at 4a (0,0,0); M, $Q1$, $Q2$ at 16e (x,x,x). [c] $D^{MM} = ((d_{M\cdots M}/d_{M-M}) - 1) \times 100$. [d] $D^{MQ} = ((d_{M-Q2}/d_{M-Q1}) - 1) \times 100$.

pressibility[39] where we could expect the largest structural effect under pressure. We show later, by DFT calculations, that $GaNb_4Se_8$ and $GaNb_4S_8$ are expected to show the same behavior. The results of the structure refinements are summarized in Table 1 together with the data for $GaNb_4Se_8$ from ref 18 for comparison. All compounds crystallize in the cubic $GaMo_4S_8$ structure (Figure 1) with tetrahedral Nb_4 or Ta_4 clusters. The distorted octahedral coordination around the Nb or Ta atoms and the connection between the M_4Q_4 cubes via the longer $M-Q2$ bonds correspond to Figure 2.

At ambient conditions, we find Ta−Ta bond lengths of 3.002(2) Å in $GaTa_4Se_8$ and similar Nb−Nb distances of 2.975(1) Å in $GaNb_4S_8$. Thus, the $M-M$ bond lengths within the M_4 cluster are almost the same in the sulfide as in the selenides, in contrast to the intercluster $M\cdots M$ distances, which are 4.085(1) Å in $GaNb_4S_8$ but 4.322(1) Å in $GaTa_4Se_8$. We define a degree of clustering as the deviation from the spinel's pyrochlore network with the ratio $D^{MM} = ((d_{M\cdots M}/d_{M-M}) - 1) \times 100(\%)$ and obtain larger values of 43-44% for the selenides than for $GaNb_4S_8$, where the intercluster distances are only 37% longer than the cluster bonds. The chalcogenide coordination polyhedra around each niobium or tantalum atom is a distorted octahedron (3m symmetry) with three shorter $M-Q1$ and three longer $M-Q2$ bonds. Again we define a degree of distortion from ideal octahedral coordination (as in the spinel type) by a quotient $D^{MQ} = ((d_{M-Q2}/d_{M-Q1}) - 1) \times 100(\%)$ and find the same values of 9.6% for $GaNb_4S_8$, $GaTa_4Se_8$, and $GaNb_4Se_8$, respectively, at ambient pressure.

The results of the high-pressure structure determinations of $GaTa_4Se_8$ are also compiled in Table 1. We observe a continuous decrease of the cubic lattice parameter from a = 10.358 Å at ambient pressure to a = 9.994 Å at 14.5 GPa. But more important are small shifts of the atomic coordinates, especially for the metal site. The parameter x(Ta) changes from 0.6025(2) at ambient pressure to 0.6036(5) at 14.5 GPa. Even though these shifts are small, they have significant effects on the atomic distances, as seen from Table 1 and in Figure 3. The short Ta−Ta bond lengths are only weakly reduced, but the Ta$\cdots$Ta intercluster distances decrease significantly from 4.322(1) to 4.137(7) Å at 14.5 GPa. Thus, the size of the Ta_4 cluster remains almost constant, but the distances to the neighboring clusters decrease with pressure. In other words, the degree of clustering decreases, but only slightly, from 44 to 41%.

Figure 3 shows also the effect of pressure on the Ta−Se bonds. The Ta−Se1 bond lengths decrease only slightly by less

(21) The relative change of distortion is defined as $\Delta D/D_0 = (D^{MM} - D_0^{MM})/D_0^{MM}$ for the metal atom clustering and $(D^{MQ} - D_0^{MQ})/D_0^{MQ}$ for the octahedral distortion.
(22) Ramirez, A. P. *Annu. Rev. Mater. Sci.* **1994**, *24*, 453.
(23) Binder, K.; Young, A. P. *Rev. Mod. Phys.* **1986**, *58*, 801.
(24) (a) Chu, C. W.; Huang, S. Z.; Lin, C. H.; Meng, R. L.; Wu, M. K.; Schmidt, P. H. *Phys. Rev. Lett.* **1981**, *46*, 276. (b) Yao, Y. S.; Guertin, R. P.; Hinks, D. G.; Jorgensen, J.; Capone, D. W., II. *Phys. Rev. B* **1988**, *37*, 5032.
(25) Perdew, J. P.; Burke, S.; Enzerhof, M. *Phys. Rev. Lett.* **1996**, *77*, 3865.
(26) In general, phonon frequencies are expected to increase under pressure due to the harder lattice.
(27) Solovyev, I. V.; Dederichs, P. H. *Phys. Rev. B* **1994**, *49*, 6736.
(28) Anisimov, V. I.; Aryasetiawan, F.; Lichtenstein, A. I. *J. Phys. Cond. Mater.* **1997**, *9*, 767.
(29) Stoe and Cie. *Stadi4 Four-Circle Diffractometer Control Program*; Darmstadt, Germany, 1977.
(30) Stoe and Cie. *X-Red data reduction, Rev. 1.19*, Darmstadt, Germany, 1999.
(31) Mao, H. K.; Bell, P. M. *Carnegie Inst. Washington Year Book* **1980**, *79*, 409.
(32) Barnett, J. D.; Block, S.; Piermarini, G. J. *Rev. Sci. Instrum.* **1979**, *50*, 1002.
(33) Stoe and Cie. *DIF4 Four-Circle Diffractometer Control Program*; Darmstadt, Germany, 1991.
(34) Alden, R.; Stewart, J. M.; Watenpaugh, K. *CRYLSQ, Xtal3.2 Reference Manual*; Hall, S. R., Flack, H. D., Stewart, J. M., Eds.; Universities of Western Australia, Geneva, and Maryland, 1992.
(35) Hall, S. R., Flack, H. D., Stewart, J. M., Eds. *Xtal3.2 Reference Manual;* Universities of Western Australia, Geneva, and Maryland, 1992.
(36) Lueken, H. *Magnetochemie*, B. G. Teubner: Stuttgart, Leipzig (Gemany), 1999.
(37) *Low Level Measurements*; Keithley Instruments, Inc.: Cleveland, Ohio, 1998.
(38) Jayaraman, A. *Rev. Mod. Phys.* **1983**, *55*, 65.
(39) Ni, B. *Pressure-Induced Superconductivity in the Semiconducting Metal-Cluster Compounds Ga(Ta,Nb)$_4$(Se,S)$_8$*; Mensch-und-Buch Verlag: Berlin, 2002, Zugl. Disssertation, Universität zu Köln, 2001.

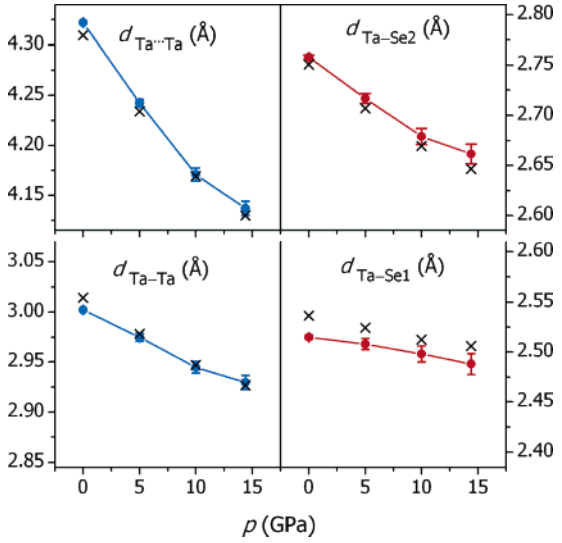

Figure 3. Variation of the Ta−Ta and Ta−Se bond lengths in $GaTa_4Se_8$ with increasing pressure. Crosses mark the data as calculated by the LAPW method.

than 0.03 Å, whereas the Ta−Se2 distance is almost 0.1 Å shorter at 14.5 GPa. Thus, the difference between the shorter and longer Ta−Se bonds decreases with increasing pressure, which means that the distortions of the $TaSe_6$ octahedra become smaller. This degree of distortion decreases from 9.6% at ambient pressure to 7% at 14.5 GPa. The consequence of such pressure-induced changes of the Ta−Ta and Ta−Se bonds is that the geometry of the Ta_4Se_4 cubes (see Figure 2a) remains almost constant (d_{Ta-Ta}, d_{Ta-Se1}) whereas the distances between them ($d_{Ta\cdots Ta}$, d_{Ta-Se2}) decrease significantly with increasing pressure. By comparing the relative changes ($\Delta D/D_0$)[21] of the octahedral distortion with that of the metal atom clustering with pressure, we find that the relative decrease of the $TaSe_6$ octahedral distortion (−27% at 14.5 GPa) is about four times larger than that of the Ta atom clustering (−6.8%). As we will show later, such an unusual change of the local structure unter high pressure strongly affects the electronic conduction (hopping) between the clusters and is connected with the occurrence of superconductivity in these materials.

3. Electrical Resistance at Ambient Pressure

The normalized electrical resistances ρ/ρ_{300K} of pressed and sintered powder samples of $GaTa_4Se_8$, $GaNb_4Se_8$, and $GaNb_4S_8$ between 8 and 320 K are shown in Figure 4. We cannot give reliable specific resistivity values because of the unknown geometry factor of the pellets and especially because we do not know the contribution of grain boundary effects to the resistance.

All compounds are semiconductors with resistance values (ρ) about 1 Ω at 320 K, which increase exponentially up to 10^6 Ω at ∼40 K for the niobium compounds, whereas in the case of $GaTa_4Se_8$ ρ reaches only ∼30 Ω at 8 K. From almost linear dependencies of $-\ln(1/\rho)$ vs T^{-1} between 320 and 250 K (see inset in Figure 4), we estimate hopping activation energies E_G of 0.16 eV for $GaTa_4Se_8$, 0.19 eV for $GaNb_4Se_8$, and 0.28 eV for $GaNb_4S_8$. The compounds show decreasing gaps to lower temperatures, which is typical for a variable range hopping (VRH) mechanism of the conductivity.

The similar resistance values of the niobium compounds clearly indicate that the long intercluster Nb···Nb distances are not the determining parameter for the strengths of the electronic conduction in these materials. Otherwise, the conductivity of $GaNb_4S_8$ with $d_{Nb\cdots Nb} = 4.085$ Å should be much better than that of $GaNb_4Se_8$ with $d_{Nb\cdots Nb} = 4.320$ Å. In any case, as long as the intercluster distances remain larger than ∼4 Å, we can truly consider the Nb_4 and Ta_4 cluster units as very weakly coupled, and the structure remains far away from the spinel-like metallic system. This also holds true for $GaTa_4Se_8$, where the intercluster Ta···Ta distance is 4.322(1) Å, and although it decreases to 4.137(7) Å at 14.5 GPa, this is still too far for a direct electronic coupling (see below). The smaller gap and the much smaller low-temperature resistance of $GaTa_4Se_8$ compared with those of the other compounds with group 5 metals indicates that the electron hopping between cluster-MOs of 5d orbitals (Ta_4) is stronger than that for 4d (Nb_4) or even 3d (V_4) due to decreasing effective hopping matrix elements.

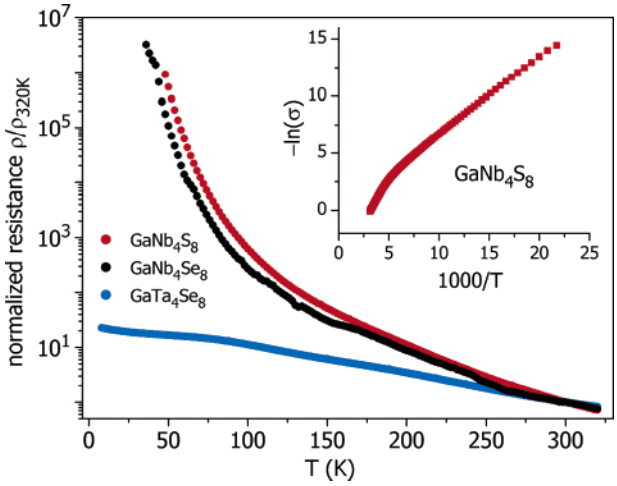

Figure 4. Temperature dependencies of the electrical resistance for $GaNb_4S_8$, $GaNb_4Se_8$, and $GaTa_4Se_8$. From the linear parts of the Arrhenius plots (shown only for $GaNb_4S_8$) we obtained activation energies of 0.28 eV ($GaNb_4S_8$), 0.19 eV ($GaNb_4Se_8$), and 0.16 eV ($GaTa_4Se_8$) at room temperature.

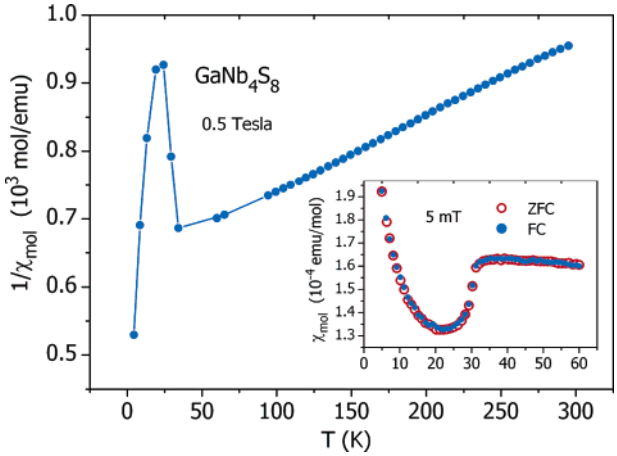

Figure 5. Magnetic susceptibility of $GaNb_4S_8$ at 0.5 T. (Inset) Zero field cooled (ZFC) and field cooled (FC) susceptibility loop measured at 5 mT.

4. Magnetic Measurements

The temperature dependence of the inverse magnetic susceptibility of $GaNb_4S_8$ is shown in Figure 5. By fitting the linear part between 300 and 120 K with a modified Curie−Weiss law, we obtain an effective magnetic moment $\mu_{eff} = 1.76 \pm 0.04\ \mu_B$

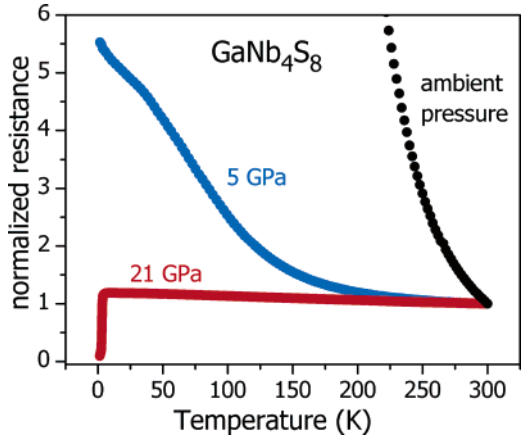

Figure 6. Temperature dependence of the normalized electrical resistance ρ/ρ_{300K} of $GaNb_4S_8$ at some selected pressures.

per formula unit, a temperature-independent part of the susceptibility $\chi_0 = 3.9 \pm 0.2 \times 10^{-4}$ emu/mol and a paramagnetic Curie temperature (Weiss constant) $\theta_{CW} = -298 \pm 13$ K. The experimental magnetic moment is in good agreement with the spin-only value of one unpaired electron per Nb_4 cluster ($\mu_{eff} = g\sqrt{S(S+1)} = 1.732$ with $g = 2$ and $S = {}^1/_2$).

The large negative value of θ_{CW} indicates strong antiferromagnetic correlations between the cluster units; one may expect antiferromagnetic order at low temperatures, but no sign for magnetic ordering is observed down to 2 K. However, we observe a sudden drop of the susceptibility at 32 K (see inset in Figure 5), then a minimum at 22 K and finally an upturn at lower temperatures, but the reason for this anomaly is not yet clear. We rule out long-range antiferromagnetic order by the neutron powder diffraction experiment, where no additional reflections occurred down to 4 K. No indication of splitting or broadening of any reflection is discernible. Thus, we can assume that the cubic symmetry of $GaNb_4S_8$ is preserved even at low temperatures and no structural distortion is responsible for the drop of the susceptibility at 32 K within the accuracy of the neutron diffraction technique.

Regarding the absence of long-range magnetic ordering, it is interesting to mention that the niobium substructure in $GaNb_4S_8$ is closely related to the pyrochlore type, which is well-known to exhibit anomalous magnetic properties.[22] The inability of such a system to satisfy all pairwise interactions and to establish long-range magnetic order is typical for frustration effects leading to cluster-glass or related behavior.[23] In the present case, we demonstrate the absence of cluster-glass ordering in $GaNb_4S_8$ by field cooled (FC) and zero field cooled (ZFC) cycles of $\chi(T)$ at low fields (5 mT, see inset in Figure 5), which reveal no significant splitting. Nevertheless, we feel that a certain kind of spin frustration effect prevents long-range magnetic ordering in $GaNb_4S_8$. The selenides show similar magnetic properties with $S \approx {}^1/_2$ and the same kind of anomalies at 35 and 55 K for $GaNb_4Se_8$ and $GaTa_4Se_8$, respectively.[39]

5. Pressure-Induced Superconductivity in $GaNb_4S_8$

Figure 6 shows the temperature dependence of the normalized resistance of $GaNb_4S_8$ at some selected pressures of ~0, 5, and 21 GPa. The slope of $\rho(T)/\rho(320K)$ decreases drastically with increasing pressure, which means a strong reduction of the activation energy. From the almost linear parts of Arrhenius plots we estimate $E_G = 0.28$ eV at ambient conditions and $E_G = 0.03$ eV at 5 GPa. Above 10 GPa, we observe a sudden drop of the resistance at a critical temperature of 2.1 K, indicating a superconducting transition. The superconducting fraction increases with pressure (granular superconductivity)[24] and amounts to more than 90% at 23 GPa. T_C increases linearly with increasing pressure from 2.1 K at 10 GPa up to 4 K at 23 GPa.

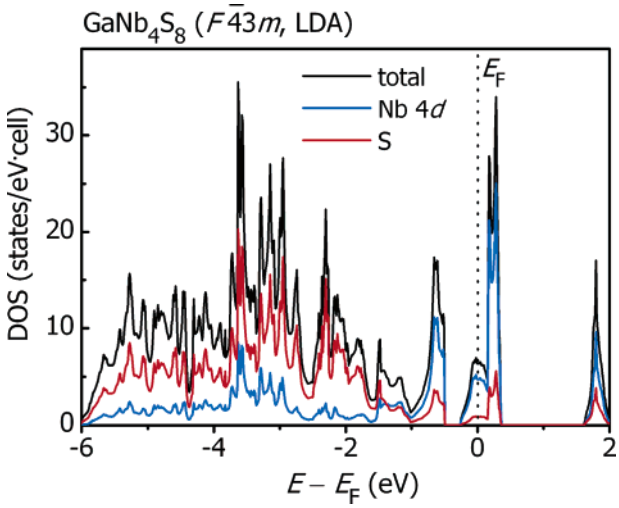

Figure 7. Density-of-states (DOS) of $GaNb_4S_8$, calculated with the LMTO method. Black: total DOS, blue: Nb 4d-, red: S 3s/3p-contribution. The energy zero is taken at the Fermi level.

We were not able to perform the Meissner-Ochsenfeld experiment, because of the necessary high-pressure conditions. Instead of this we proved the superconductivity by measuring the magnetic field dependence of T_C. The transition temperature decreases linearly with increasing field, as typical for superconducting transitions. The upper critical fields are estimated to $B_{c2} = 3.8$ T at 18 GPa and $B_{c2} = 4.5$ T at 23 GPa. Altogether, the superconductivity in $GaNb_4S_8$ is very similar to that in $GaNb_4Se_8$ and $GaTa_4Se_8$,[20] but the transition temperatures are higher in the selenides (up to 8 K for $GaTa_4Se_8$) than in the sulfide reported here. This may be traced back to the higher ionicity of the Nb−S bonds compared with that of the Nb−Se or Ta−Se bonds, which is connected with a smaller electronic coupling of the metal atoms via S or Se bridges.

6. Electronic Structure

LMTO (LDA) Calculations. To get an overview of the electronic structure and bonding characteristics, we have performed LDA calculations first with the fast LMTO method. We confine the description on $GaNb_4S_8$, because we found similar electronic features for $GaNb_4Se_8$ and $GaTa_4Se_8$. The total density of states (DOS) together with the contributions of the Nb 4d orbitals and the sulfur atoms is displayed in Figure 7. The Fermi level (E_F) lies within a region of relatively high values of DOS, indicating that $GaNb_4S_8$ should be a metal in contradiction with the experimental results.

At this point, we may accept this as an artifact of the calculation, which we will overcome later. Thus far, this result is expected from the idea of very weakly coupled cluster-MOs (Figure 2b), whose t_2 levels produce partially occupied, flat bands around E_F. Thus, the band structure looks like that of a metal, but we must keep in mind that the existence of partially occupied bands is not a sufficient condition for a metallic state.

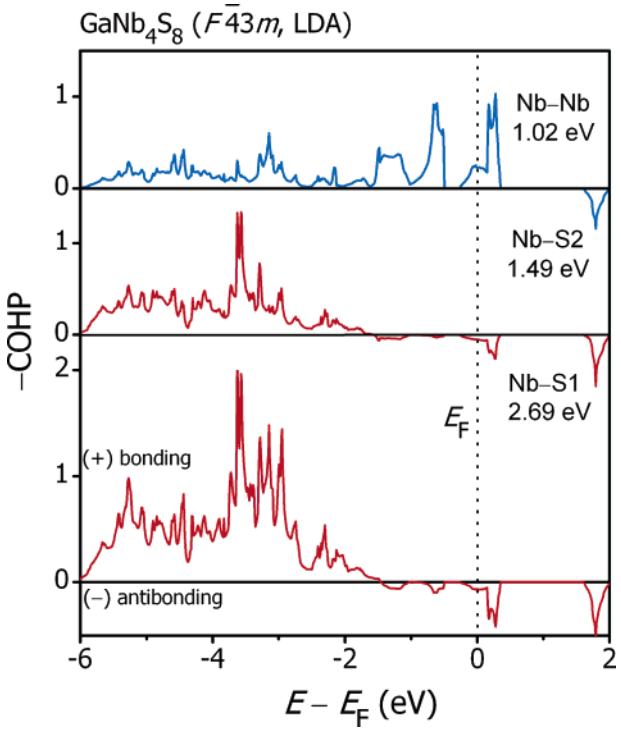

Figure 8. Crystal Orbital Hamilton population (COHP) diagrams of selected bonds in $GaNb_4S_8$. The ICOHP bonding energy is given in eV for each bond.

In fact a certain slope of the bands, respectively Fermi speed $v_F = (dk/dE)_{E=E_F}$ is also an important precondition to achieve delocalization. The latter condition is not fulfilled in $GaNb_4S_8$, where the bands are much too flat and produce therefore the DOS peak around E_F. The part of the DOS between +0.3 eV and −0.3 eV is exactly one-sixth-filled and corresponds to the bands generated by the t_2 orbitals of the cluster-MO. The lower peak between −1 and −0.5 eV represents the completely filled orbitals with *e* symmetry (see Figure 2b). Even though the LMTO calculation produces a nonmagnetic metallic ground state instead of the correct magnetic insulator, the results support the idea of weakly coupled cluster orbitals, and they can be used to explore some bonding characteristics by the COHP method.

Figure 8 shows the COHP diagrams of the Nb−Nb and Nb−S bonds in $GaNb_4S_8$. The Nb−S bonding states are completely filled and located considerably below the Fermi level. The ICOHP bonding energy of the shorter Nb−S1 bond in the Nb_4S_4 cube (2.69 eV) is about 80% larger than the Nb−S2 bond (1.49 eV) that connects the cubes. The region around the Fermi energy is clearly dominated by the niobium 4d orbitals (Nb−Nb bonding states), which are not completely filled up to E_F. The integration yields a ICOHP bonding energy of 1.02 eV/bond. The strong Nb−Nb bonding states are only slightly mixed with the Nb−S states in the vicinity of the Fermi level, as seen from the weak Nb−S antibonding character and the small contribution of the sulfur orbitals at E_F (see Figure 7). Although the LMTO calculations have not produced the physically correct ground state, we can recognize significant differences of the Nb−S1 and Nb−S2 bond strengths in $GaNb_4S_8$ and that the character of the density-of-states at E_F is strongly dominated by the Nb−Nb bonding states of the weakly coupled Nb_4 cluster units

LAPW (GGA) Calculations. Next we performed more accurate full potential LAPW calculations of $GaNb_4S_8$, $GaNb_4Se_8$, and $GaTa_4Se_8$ using a GGA functional[25] to approximate the exchange correlation energy. The resulting density-of-states are almost identical to those obtained from the LMTO calculations and are therefore not shown. However, this method allows geometry optimizations by minimizing the Hellmann-Feynman forces in an iterative process. In this way we are able to prove the changes of the internal structure of $GaTa_4Se_8$ with increasing pressure theoretically by optimizing the geometries for different unit cell volumes and comparing the equilibrium states with the experimental data from the high-pressure X-ray measurement. The calculated geometries are in good agreement with the experimental data. To illustrate this, we have marked the calculated bond lengths of $GaTa_4Se_8$ in Figure 3. All theoretically calculated distances lie within twice the standard deviations of the high-pressure X-ray data.

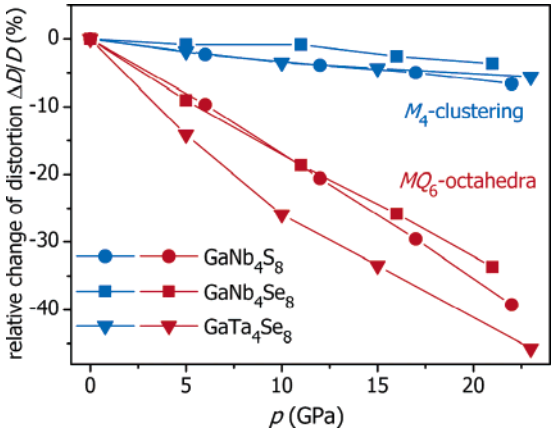

Figure 9. Calculated relative changes the structural distortions for $GaNb_4Se_8$, $GaNb_4S_8$, and $GaTa_4Se_8$ with increasing pressure.[21] Blue markers are the change of *M* atom clustering, red markers show the change of the MQ_6 octahedral distortion.

This result shows, that we can obtain reliable structural data from the LAPW calculation. We have also calculated the high-pressure structural behavior of $GaNb_4Se_8$ and $GaNb_4S_8$ and obtained results similar to those of $GaTa_4Se_8$. Under high pressure, the niobium compounds show also a continuous decrease of the NbQ_6 octahedral distortion and the metal atom clustering. These changes are summarized in Figure 9, where the calculated relative changes of the distortions $\Delta D/D_0$ for all three compounds are displayed. In all cases, the metal atom clustering D^{MM} decreases only about −6% at 20 GPa, but the relative decrease of the MQ_6 distortion D^{MQ} reaches up to −40% at 20 GPa. In addition, the latter is largest for $GaTa_4Se_8$, which agrees with the higher compressibility of the tantalum compound,[39] whose lattice is obviously softer.

It is interesting to note that the onset of superconductivity at about 10 GPa is at noticeably higher T_C in $GaTa_4Se_8$ (T_C = 5.8 K),[20] whereas it occurs almost at the same and lower temperatures in $GaNb_4Se_8$ (T_C = 2.4 K)[20] and $GaNb_4S_8$ (T_C = 2.1 K), which show very similar structural changes under pressure. These structural changes are expected to be associated with a modification of the phonon spectrum, which is one important parameter for the occurrence of superconductivity. Indeed, we have found one intense Raman mode in $GaTa_4Se_8$,[20] whose frequency decreases strongly with pressure[26] and reaches saturation at about 10 GPa, which just coincides with the onset of superconductivity. We suspect that the appearance of this soft mode is connected with the onset of superconductivity in

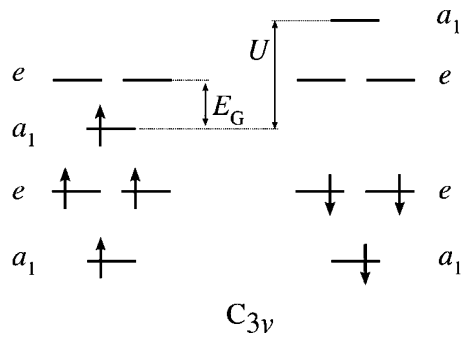

Figure 10. Spin polarized MO model of a Nb_4 cluster with C_{3v} symmetry. The orbitals which generate the "lower Hubbard band" (left) and the "upper Hubbard band" (right) are depicted. U splits the highest occupied a_1 level, and the insulating energy gap E_G occurs between the occupied a_1 and the empty e levels. The resulting spin moment is $S = {}^1/_2$.

$GaTa_4Se_8$, and this is, by regarding their similar structural behavior, also most probable for the niobium compounds $GaNb_4S_8$ and $GaNb_4Se_8$.

LAPW (LDA+*U*) Calculations. At last we want to achieve the correct insulating magnetic ground state from the band structure calculations. One possible way to overcome the difficulties arising from Coulomb repulsion is the introduction of the Hubbard U in the calculations. By this so-called LDA+U method we split certain electronic levels in "lower" and "higher" Hubbard bands with the insulating gap between them. To our knowledge, this was never done for metal cluster compounds, and the most experiences so far are from materials with 3d metals. However, the cluster-MO is the key to obtain the insulating gap, but this cannot occur as long as the highest MO (t_2) is three-fold degenerate. We had to reduce the symmetry to lift this degeneracy and chose a minimal subgroup of index 2, which is represented by the space group $R3m$. The point group of the cluster-MO is now C_{3v} and the three-fold degenerated t_2 level splits into one single a_1 and a two-fold degenerated e level.

When U is applied, we expect a splitting of the highest occupied a_1 levels, generating the "lower" and "upper" Hubbard levels, as depicted schematically in Figure 10. An energy gap should arise between the occupied lower a_1 and the empty e levels, whereas the rest of the cluster-MO should remain almost unaffected.

The result of the spin-polarized LDA+U band structure calculation as shown in Figure 11 confirms the preceding assumptions. A ferromagnetic approach was used, although the magnetic data show antiferromagnetic correlations. However, because of the absence of magnetic ordering, any artificial antiferromagnetic model would not be better than the simpler ferromagnetic one. We find an energy gap E_G of ~0.2 eV between the upper and lower Hubbard bands. Our calculations required a rather large U of 6 eV to produce a gap which corresponds approximately to the experimental value of E_G = 0.28 eV. Expected U values for free Nb ions are around 3 eV,[27] but the values for U depend also strongly on the chemical environment.[28] However, the results of LDA+U are usually checked by the predicted value of the magnetic moment. In our case, we calculate exactly one unpaired spin per Nb_4 cluster ($\mu_{eff,calc}$ = 1.73 μ_B), which is in excellent agreement with the experimental value for $GaNb_4S_8$ of 1.76 μ_B ($S = {}^1/_2$). This correct magnetic moment was already achieved with much smaller values for U of 3-4 eV, but a gap discerns only with $U \geq 4$ eV. Here we must keep in mind that DFT calculations

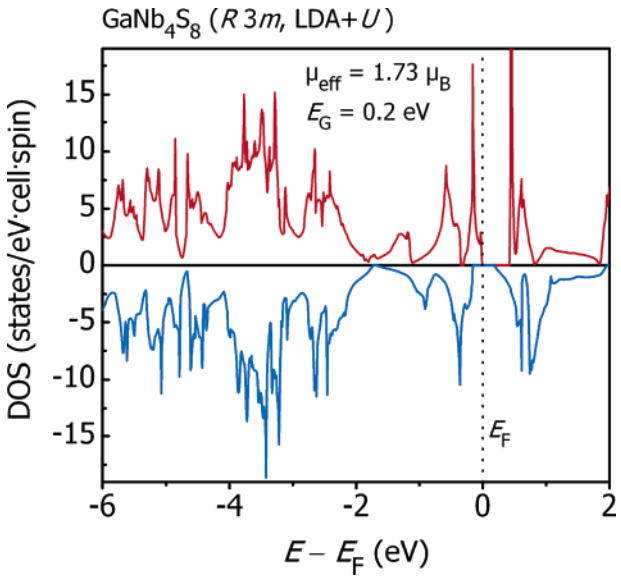

Figure 11. Spin polarized total density-of-states of $GaNb_4S_8$, calculated with the LDA+U approach (U = 6 eV). An energy gap of ~0.2 eV discerns between the "upper" and "lower" Hubbard bands. The calculated magnetic moment is exactly one spin per Nb_4 or μ_{eff} = 1.73 μ_B, respectively.

generally underestimate energy gaps and also that we deal with very small values of 0.2-0.3 eV. Thus, the physical value of the Coulomb parameter U is rather expected to be around 3-4 eV.

Subsequent LDA+U calculations with $GaNb_4Se_8$ and $GaTa_4Se_8$ revealed similar activation energies E_G between 0.2 and 0.3 eV and magnetic moments about 1.73 μ_B. This is somewhat too large in the case of $GaTa_4Se_8$, where the experimental moment is only 0.7−0.9 μ_B.[39] However, apart from the exact values of E_G and the magnetic moments, the most important result is that we have achieved physically correct insulating magnetic ground states for materials with $GaMo_4S_8$ structure for the first time. The insulating gap occurs within the cluster-MO between the occupied and unoccupied $M-M$ bonding states and is therefore highly sensitive to any distortion of the M_4 tetrahedra. In other words, we can expect strong electron-phonon coupling, which clearly plays an important role for the occurrence of superconductivity.

7. Conclusion

We have performed experimental and theoretical investigations of the tetrahedral cluster compounds $GaNb_4S_8$, $GaNb_4Se_8$, and $GaTa_4Se_8$ with the $GaMo_4S_8$-type structure. This new class of Mott insulators exhibits electronic conduction by hopping of localized unpaired spins ($S = {}^1/_2$) between separated clusters with activation energies between 0.15 and 0.3 eV at ambient pressure. No magnetic order could be detected down to 2 K despite strong antiferromagnetic correlations. The insulating gaps decrease under pressure, and at $p \approx 10$ GPa we find transitions to superconductivity in $GaNb_4S_8$ with T_C up to 4 K. We believe that the superconductivity in these materials is connected to a gradual decrease of the distortion of the MQ_6 octahedra, which we could prove experimentally by high-pressure X-ray diffraction for $GaTa_4Se_8$ and also by quantum chemical calculations for $GaNb_4S_8$ and $GaNb_4Se_8$. The DFT band structure calculations also show that the properties of these materials are determined by localized and highly correlated

electronic states in the vicinity of the Fermi level that results from the weak coupling of the cluster-MO. By using the LDA+U method, we could achieve a physically correct description of the insulating magnetic ground state of these materials with activation energies and magnetic moments in good agreement with the experimental values.

8. Experimental Section

Sample Preparation and Characterization. Polycrystalline samples of $GaNb_4S_8$, $GaNb_4Se_8$, and $GaTa_4Se_8$ up to 1000 mg were prepared by heating stoichiometric mixtures of the elements (all purities > 99.5%) at 1123−1223 K in a purified argon atmosphere using alumina crucibles in silica ampules. To avoid bursting the ampules due to exothermic reactions of the elements, we increased the temperature with a rate of 50 K/h up to 1123 K in the first heating runs, keeping this temperature for 15 h, followed by cooling with 300 K/h. The resulting black powders, mainly consisting of the niobium or tantalum dichalcogenides, were homogenized using an agate mortar in an argon-filled glovebox. Two to three subsequent heating runs at 1223 K for 15 h yielded black polycrystalline samples of the desired compounds, which showed no decomposition when exposed to air. The purity was checked by comparing their X-ray powder patterns (Stoe StadiP, 7° PSD detector, Cu Kα_1 radiation, λ = 1.54056 Å, Si as external standard) with those calculated from the single-crystal data. No impurities could be detected within the accuracy of the X-ray powder method. Small single crystals of about 50−80 μm were selected from the powder samples and checked for their quality by Laue photographs.

Single-Crystal X-ray Methods. X-ray structure determinations were performed with single crystals of $GaNb_4S_8$ and $GaTa_4Se_8$ using a Stoe Stadi4 four-circle diffractometer (Mo Kα radiation, graphite monochromator, λ = 0.71069 Å, ω/ϑ scan, $3° \le \vartheta \le 40°$). Absorption effects were corrected empirically by collecting Ψ-scan data of suitable reflections. The Stadi4[29] software was used for data collection, and X-Red,[30] for absorption corrections and data processing. To perform structure determinations of $GaTa_4Se_8$ under high pressure, the diffractometer has been equipped with a special diamond-anvil cell (Mao-Bell type DAC)[31] using liquid nitrogen as pressure medium and the shift of the ruby fluorescence lines at 692.70 and 694.25 nm for pressure determination.[32] A modified DIF4[33] software was used for data collection to collect the maximum amount of reachable data (about 40% of the reciprocal space). The absorption of the DAC was determined empirically and applied to the data. Very strong reflections originating from the diamonds were removed manually. Structure refinements against F_o were performed with the CRYLSQ[34] routine of the XTAL3.2[35] program package.

Magnetic Measurements. Magnetic moment measurements were done on polycrystalline samples (20-40 mg) with a SQUID magnetometer (MPMS-XL5) in the temperature range (2 ± 0.01)-(300 ± 1.5) K with magnetic flux densities between 10^{-3} and 5 T. Measured susceptibilities were corrected for the sample container (gelatin capsules) and holder (straws) and also for the diamagnetic contributions of the constituent atoms.[36] Effective magnetic moments were calculated by fitting the corrected molar magnetic susceptibility data χ_m with the equation

$$\chi_m = \chi_0 + \frac{C}{T - \theta_{CW}}$$

where θ_{CW} is the paramagnetic Curie-Weiss temperature (Weiss constant) and χ_0 is a temperature-independent part of the susceptibility.

Electrical Resistance Measurements. Measurements of electric resistances were performed using the standard four-probe dc method with pressed (40 kN) and sintered (973 K) pellets (∅ 6 mm) between 8 and 320 ± 0.1 K. A Keithley 2400 current source and Keithley 2182 nanovoltmeter were used in the current reversal mode.[37] Applied dc intensities were 1-10 μA.

Resistance measurements under high pressure were performed with a Merrill-Basset type DAC.[38] Four gold wires (∅ 25 μm) were fixed mechanically to small sintered pieces of the samples in the hole (∅ 250 μm) of the gasket (Inconel 750). Liquid argon was used as pressure medium. Additional resistance measurements under pressure were performed with applied transversal magnetic fields up to 8 T. For further details about the high-pressure resistance measurements see ref 39.

DFT Band Structure Calculations. Self-consistent DFT band structure calculations for $GaTa_4Se_8$, $GaNb_4Se_8$, and $GaNb_4S_8$ were performed with the linear-muffin-tin-orbital (LMTO) method in its scalar-relativistic version. LMTO makes use of the atomic sphere approximation (ASA). This implies ascribing to every atom in the structure a region bounded by the Wigner-Seitz sphere in such a way that the sum of the sphere volumes is identical to that of the unit cell. The electronic potential and the charge distribution are spherically symmetric within these spheres. The ASA has the large drawback that that there is no way to fix the radii for the same atom types in different structures or geometries. Thus, no reliable geometry optimizations are possible with this method. The program package TB-LMTO-ASA[40,41] was used together with the COHP[42] extension implemented by Boucher.[43] Sets of 91 irreducible k points (grid 11 × 11 × 11, space group $F\bar{4}3m$) were used for reciprocal space integrations by the tetrahedron method. The basis sets consisted of Ga-3s/3p/[3d], Ta-6s/6p/5d/[4f], Nb-5s/5p/4d/[4f], S-3s/3p/[3d] and Se-4s/4p/[4d] orbitals. ("downfolded" orbitals are in brackets). All SCF iterations converged to total energy changes smaller than 10^{-5} Ryd. The crystal orbital Hamilton population (COHP) method was used for the bond analysis. COHP gives the energy contributions of all electronic states for a selected bond. Since the values are negative for bonding states, we plotted −COHP(E) to get positive values according to the well-known COOP diagrams.

Although the results obtained by the LMTO method turned out to be reasonable, we used full-potential LAPW band structure calculations to avoid any problems caused by the ASA and especially to optimize the atomic coordinates in the unit cells. Full-potential LAPW is based on the muffin-tin construction with nonoverlapping spheres. Within these spheres of radius $r_{mt,\alpha}$ (α = atom type) the angular dependence of the potential $V_\alpha(r)$ is expanded in spherical harmonics

$$V_\alpha(r) = \sum_{lm^i} V_{\alpha l m_l}(r) Y_l^{m_l}(\hat{r}) \quad \text{for } r < r_{mt,\alpha}$$

In the interstitial region between the spheres the potential is represented by a plane wave expansion

$$V(r) = \sum_{K_n} V_{K_n} \exp iK_n r$$

with K_n the reciprocal lattice vectors. Because of the great flexibility and accuracy of this expansion for the potential and charge density, a very high numerical accuracy is achieved for the LAPW method. Further technical details can be found in ref 46 and the monograph of *Singh*.

To obtain theoretical equilibrium geometries for the cubic structures of $GaTa_4Se_8$, $GaNb_4Se_8$, and $GaNb_4S_8$ with cell volumes corresponding to pressures of 5, 10, and 14.5 GPa, we performed LAPW calculations using the WIEN2k program package.[45,46]All atomic positions were

(40) Andersen, O. K.; Jepsen, O. *Tight-Binding LMTO*, ver. 47c; Max-Planck-Institut für Festkörperforschung: Stuttgart, Germany, 1994.
(41) Skriver, H. L. *The LMTO method: muffin-tin orbitals and electronic structure*; Springer: Berlin, New York, 1984.
(42) Dronskowski, R.; Bloechl, P. E. *J. Phys. Chem.* **1993**, *97*, 8617.
(43) Boucher, F.; Rousseau, R. *Inorg. Chem.* **1998**, *37*, 2351.
(44) Singh, D. J. *Planewaves, Pseudopotentials and the LAPW Method*; Kluwer Academic Publishers: Boston, Dordrecht, London, 1994.
(45) Blaha, P.; Schwarz, K.; Madsen, G. K. H.; Kvasnicka, D.; Luitz, J. *WIEN2k-An Augmented Plane Wave + Local Orbitals Program for Calculating Crystal Properties*; TU Wien: Vienna, Austria, 2001.
(46) Schwarz, K.; Blaha, P. *Comput. Mater. Sci.* **2003**, *28*, 259.

relaxed by using a dampened Newton scheme, based on the minimization of Hellmann-Feynman forces to values smaller than 0.5 mRyd/au. The total energies and charge densities of the preceding SCF cycles converged to changes smaller than 10^{-4}. The basis sets consisted of about 2320 plane waves (depending on the volume) up to a cutoff $R_{mt}K_{max} = 8.0$ and 242 local orbitals. The atomic sphere radii R_{mt} were 2.0 (Ga), 2.2 (Nb, Ta) and 2.0 au (S, Se). Twenty k points ($7 \times 7 \times 7$ mesh) were used in the irreducible wedge of the cubic Brillouin zone.

To reproduce the correct magnetic insulating ground states, we used the LDA+U approach to implement the WIEN2k program. A value of 6 eV was used for the Hubbard U, which makes the energy of a level ϵ_i dependent on its degree of occupation n_i, according to $\epsilon_i = \epsilon_{i,LDA} + U(^1/_2 - n_i)$. Trigonal symmetry with space group $R3m$ in a pseudocubic cell ($\alpha_{rh} = 60°$) was used for this calculation. The atomic sphere radii were the same as in the cubic case, the typical basis sets consisted of 2267 plane waves up to a cutoff $R_{mt}K_{max} = 8.0$ and 242 local orbitals. Forty-four k points ($7 \times 7 \times 7$ mesh) were used in the irreducible wedge of the trigonal Brillouin zone.

Acknowledgment. We are indebted to Anette Imre for valuable help with the high-pressure X-ray experiments and to Winfried Kockelmann (RAL/ISIS) for the opportunity to perform neutron diffraction experiments. M. M. A. thanks D. I. Khomskii for useful discussions. This work was supported financially by the Deutsche Forschungsgemeinschaft through the Project Jo257/2 and SFB 608.

Supporting Information Available: X-ray crystallographic information for $GaNb_4S_8$ and $GaTa_4Se_8$ in CIF format. Neutron diffraction patterns of $GaNb_4S_8$ at 4 and 298 K; figures of the pressure and magnetic field dependencies of T_C in $GaNb_4S_8$. This material is available free of charge via the Internet at http://pubs.acs.org.

JA050243X